

# Decoupled Piecewise Linear Power Flow and Its Application to Under Voltage Load Shedding

Mang Jiang<sup>1</sup>, Qinglai Guo<sup>1</sup>, Senior Member, IEEE, Hongbin Sun, Fellow, IEEE, and Huaichang Ge

**Abstract**—Various optimizations in power systems based on the AC power flow model are inherently mixed-integer nonlinear programming (MINLP) problems. Piecewise linear power flow models can handle nonlinearities and meanwhile ensure a high accuracy. Then, the MINLP problem can be turned into a tractable mixed-integer linear programming (MILP) problem. However, piecewise linearization also introduces a heavy computational burden because of the incorporation of a large number of binary variables especially for large systems. To achieve a better trade off between approximation accuracy and computational efficiency, this paper proposes a model called decoupled piecewise linear power flow (DPWLPF) for transmission systems. The P-Q decoupling characteristic is used to ease the evaluation of the piecewise cosine functions in the power flow equations. Therefore, in optimizations, the coupling between variables is reduced. Moreover, an under voltage load shedding (UVLS) approach based on DPWLPF is presented. Case studies are conducted for benchmark systems. The results show that the DPWLPF facilitates the solution of optimal power flow (OPF) and UVLS problems much better than conventional piecewise models. And DPWLPF still enhances the approximation accuracy by using the decoupled piecewise modeling.

**Index Terms**—Integer programming, piecewise linearization, power flow modeling, under voltage load shedding.

## NOMENCLATURE

### A. Indices and Sets

$i, j/\mathcal{I}$	Index/set of the buses.
$ij/\mathcal{B}$	Index/set of the branches.
$g/\mathcal{G}$	Index/set of the units.
$z/\mathcal{Z}$	Index/set of the feeders.
$c/\mathcal{C}$	Index/set of the contingencies.
$\mathcal{I}_i$	Set of buses connected to bus $i$ .
$k$	Index of breakpoints or segments for piecewise linearization.

### B. Parameters

$g_{ij}/b_{ij}/x_{ij}$	Conductance/susceptance/reactance of branch $ij$ .
------------------------	--

$b_{ij}^l/b_i^{\text{SH}}$	Shunt susceptance of branch $ij$ /bus $i$ .
$T_{ij}/\phi_{ij}$	Tap ratio/phase shift angle of branch $ij$ .
$\underline{\theta}_{ij}/\bar{\theta}_{ij}$	Lower/upper bound of the domain set for piecewise linearization.
$\theta_{ij,k}$	Angle difference of breakpoint $k$ for branch $ij$ .
$N/N_b/N_K$	Number of buses/branches/segments.
$\underline{P}_g/\bar{P}_g$	Minimum/maximum power output of unit $g$ .
$\underline{Q}_g/\bar{Q}_g$	Minimum/maximum reactive power output of unit $g$ .
$P_i^0/Q_i^0$	Base active/reactive power demand of bus $i$ .
$P_z^{\text{shed},0}/Q_z^{\text{shed},0}$	Base active/reactive power demand of feeder $z$ for load shedding.
$a_i^Z, a_i^I, a_i^P$	Proportion coefficients of bus $i$ for ZIP load modeling.
$\underline{V}_i/\bar{V}_i$	Minimum/maximum voltage limit of bus $i$ .
$S_{ij}$	Transmission capacity of branch $ij$ .
$C_z$	Load shedding cost of feeder $z$ .
$\lambda^{\text{req}}$	Load margin requirement after a contingency.

### C. Variables

$w_{ij,k}$	Coefficients of breakpoint $k$ for branch $ij$ .
$u_{ij,k}$	Variable indicating whether the angle difference of branch $ij$ is located at segment $k$ .
$\theta_{ij}^{\text{PW}}$	Voltage angle difference of branch $ij$ for the decoupled piecewise linear modeling.
$V_i^c/\theta_{ij}^c$	Voltage magnitude of bus $i$ /voltage angle difference of branch $ij$ under contingency $c$ .
$P_i/Q_i$	Active/reactive nodal power injection of bus $i$ .
$P_i^D/Q_i^D$	Active/reactive power demand of bus $i$ .
$P_{ij}^c/Q_{ij}^c$	Active/reactive power flow of branch $ij$ under contingency $c$ .
$P_g^c/Q_g^c$	Active/reactive power output of unit $g$ under contingency $c$ .
$x_z^c$	Variable indicating the load shedding strategy of feeder $z$ under contingency $c$ .
$\lambda^c/\lambda^{\text{UVLS},c}$	Post-fault load margin without/with UVLS under contingency $c$ .

## I. INTRODUCTION

THE power flow model is the cornerstone of power network analysis. Applications such as planning, scheduling, control and reliability analysis have been implemented based on the power flow model to ensure the safety and economy of power grids. Nevertheless, the inherent nonlinearity and nonconvexity pose challenges to related problems. Because of some discrete operations and devices in power grids, optimization problems using an AC model are normally solved by

Manuscript received November 6, 2019; revised January 13, 2020; accepted January 20, 2020. Date of online publication February 13, 2020; date of current version June 15, 2020. This work was supported by China Postdoctoral Science Foundation (2020M670325).

M. Jiang (ORCID: <https://orcid.org/0000-0002-4725-2593>), Q. L. Guo (corresponding author, e-mail: [guoqinglai@tsinghua.edu.cn](mailto:guoqinglai@tsinghua.edu.cn); ORCID: <http://orcid.org/0000-0003-1435-5796>), H. B. Sun and H. C. Ge are with the Department of Electrical Engineering, State Key Laboratory of Power Systems, Tsinghua University, Beijing 100084, China.

DOI: 10.17775/CSEEJPES.2019.02900

mixed-integer nonlinear programming (MINLP) approaches. MINLP problems are non-deterministic polynomial time (NP)-hard problems and rather difficult to solve. Discrete optimal power flow (OPF) problems are intractable for commercial MINLP solvers in some cases [1]. The global optimal solution cannot be guaranteed theoretically for MINLP [2].

Linearizing the AC model is an effective solution. Thus, the original MINLP is turned into mixed-integer linear programming (MILP). Existing solvers and algorithms can guarantee a reliable and an efficient solution [3]. The DC power flow model is a well-known linearized version and is widely applied in practice [4]. However, the DC model sacrifices the ability to evaluate the voltage and reactive power, possibly leading to AC infeasibility decisions [5].

Therefore, it is desirable to retain the voltage and reactive power in linearized models. Voltage-related challenges remain serious in power systems with the growing presence of renewable generation resources and power electronic equipment [6]–[8]. Estimating the voltage and reactive power is essential to avoid voltage-induced security risks, such as cascading trip-offs of wind turbine generators [9] and commutation failures of high-voltage direct current (HVDC) systems. Linear power flow models, considering voltage and reactive power, have recently attracted increasing attention. Empirical linear models were proposed in [10]–[12] by a mathematical approximation of the power flow equations in polar coordinates. A flat voltage profile and zero angle differences across the branches were the common assumptions. Moreover, there have been some data-driven linear models. A linear model was presented in [13] using the regression approach. The optimal linearization point can be obtained by approximating a generalized moment problem [14]. Sufficient prior data are required to ensure the validity of the approximation.

All the above models are essentially a global linearization. Because of their nonlinear nature, especially for voltage and reactive power, their accuracy is limited under large perturbations. When the system states violate the common assumptions or historical distribution, the approximation deteriorates. In addition, ignoring higher order terms leads to lossless networks [11]. The network loss cannot be evaluated. The obtained locational marginal prices based on the linear model may include unacceptable outliers [1]. For the unit commitment (UC) problem, the scheduling obtained by the linear models can deviate a lot from the optimal solution [15]. It is necessary to provide accurate pictures of the system's state to avoid possible adverse effects due to considerable approximation errors.

Thus, piecewise linear power flow models [2], [3], [5], [16] were proposed to improve the accuracy at the cost of modeling complexity. Nevertheless, the optimizations are still tractable MILP problems. Reference [2], [3] approximated the quadratic terms of the phase angle differences by piecewise linear modeling using a binary expansion discretization approach. Reference [16] approximated the fictitious losses in the DC model by the piecewise modeling of the cosine functions. Reference [5] similarly approximated the cosine functions while retaining the voltage and reactive power. However, extra binary variables, along with auxiliary constraints, are

introduced, leading to an expanded search space. These binary variables are necessary to ensure the accuracy because of the non-convexity of power flow equations [5]. The number of introduced binary variables is proportional to the number of branches. For large systems, the computational burden can be heavy. Therefore, the scalability issue of piecewise methods is a concern.

To facilitate the optimizations based on piecewise linearization, this paper presents a decoupled piecewise linear power flow (DPWLPF) model for transmission networks. A decoupled modeling method to lower the complexity of piecewise linearization is proposed. Unlike conventional methods, only the active nodal power injections are utilized to estimate the angle differences for the piecewise linearization. The effects of reactive power injections on the approximated cosine functions are omitted. Therefore, the coupling between binary and state variables is reduced.

Moreover, an under voltage load shedding (UVLS) approach to prevent static voltage instability is proposed based on DPWLPF. UVLS is the last resort to maintain voltage stability in critical situations [17]. Reference [18] proposed a UVLS method by controlling smart appliances. Reference [19] solved an optimization problem to determine the location and amount of load shedding considering load uncertainties. However, most of the load cannot be continuously and precisely shed. In practice, all the load at a feeder will be shed when the relay control of the feeder receives the signal. Hence, binary variables should be included to describe their discrete characteristics. Employing the proposed DPWLPF can convert the original MINLP UVLS problem into MILP. In addition, the decoupled piecewise modeling method can mitigate computational challenges.

The contributions of this paper are two-fold: 1) A piecewise linear power flow model called DPWLPF is presented for transmission systems. The reactive power nodal injections and approximated cosine functions are decoupled to simplify piecewise linearization. Moreover, the square of the voltage magnitude is used as the independent variable in DPWLPF to enhance the approximation accuracy. 2) A MILP-based UVLS approach is proposed to improve the post-fault load margin (LM) and avoid static voltage instability. UVLS strategy is obtained periodically by solving optimizations for every severe contingency. The ZIP load model is considered and linearized in the framework of DPWLPF.

The remainder of the paper is organized as follows. Section II introduces the detailed formulations of DPWLPF. Section III presents the UVLS approach. Case studies are conducted in Section IV to verify the effectiveness of DPWLPF and UVLS. Finally, Section V presents the concluding remarks.

## II. DECOUPLED PIECEWISE LINEAR POWER FLOW

The AC power flow model is introduced first in this section. Then, the DPWLPF model is presented in detail.

### A. AC Power Flow Basics

According to the branch model shown in Fig. 1, the general formulation of the AC active and reactive power flow equations

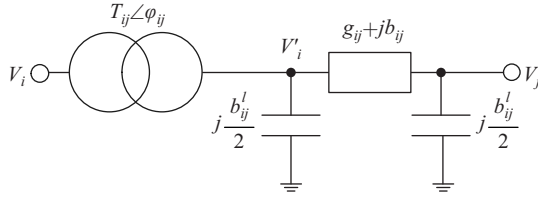


Fig. 1. A general branch model with an ideal phase-shifting transformer.

at each bus in polar coordinates is derived as:

$$P_i = \sum_{j \in \mathcal{I}_i} P_{ij}, \quad \forall i \in \mathcal{I}, \quad (1)$$

$$Q_i = \sum_{j \in \mathcal{I}_i} Q_{ij} - b_i^{\text{SH}} V_i'^2, \quad \forall i \in \mathcal{I}, \quad (2)$$

where  $b_i^{\text{SH}}$  denotes the shunt susceptance at bus  $i$ . The detailed expressions of the power flows from  $i$  to  $j$  are:

$$P_{ij} = g_{ij}(V_i'^2 - V_i'V_j \cos \theta'_{ij}) - b_{ij} V_i'V_j \sin \theta'_{ij}, \quad (3)$$

$$Q_{ij} = -b_{ij}(V_i'^2 - V_i'V_j \cos \theta'_{ij}) - g_{ij}V_i'V_j \sin \theta'_{ij} - b_{ij}^l V_i'^2 / 2. \quad (4)$$

The coupling of the transformer gives:

$$V_i' = V_i / T_{ij}, \quad \theta'_{ij} = \theta_{ij} - \phi_{ij}. \quad (5)$$

Note that the shunt conductance is omitted here because the conductance is generally negligible compared with the shunt susceptances  $b_i^{\text{SH}}$  and  $b_{ij}^l / 2$ .

### B. Model of DPWLPF

Under the classic assumption (flat voltage profiles and very small voltage angle differences),

$$V_i' \approx V_j \approx 1, \quad \theta'_{ij} \approx 0, \quad (6)$$

the sine term is approximated as:

$$V_i'V_j \sin \theta'_{ij} \approx \theta'_{ij}. \quad (7)$$

Considering  $V_i'V_j$  and  $\cos \theta'_{ij}$  as independent variables, the first-order Taylor series expansion of the cosine term is:

$$V_i'V_j \cos \theta'_{ij} \approx V_i'V_j + \cos \theta'_{ij} - 1. \quad (8)$$

Since the voltage difference across a branch is small, the bilinear term  $V_i'V_j$  can be approximated as:

$$V_i'V_j = [(V_i'^2 + V_j^2) - (V_i' - V_j)^2] / 2 \approx (V_i'^2 + V_j^2) / 2. \quad (9)$$

By substituting (7)–(9) into (3) and (4), the branch flow equations are approximated as:

$$P_{ij} = g_{ij}(V_i'^2 / 2 - V_j^2 / 2 - \cos \theta'_{ij} + 1) - b_{ij} \theta'_{ij}, \quad (10)$$

$$Q_{ij} = -b_{ij}(V_i'^2 / 2 - V_j^2 / 2 - \cos \theta'_{ij} + 1) - g_{ij} \theta'_{ij} - b_{ij}^l V_i'^2 / 2. \quad (11)$$

It can be observed that if  $\cos \theta'_{ij}$  is ignored, the expression in the approximated power flow equations (1), (2), (10) and (11) become linear considering  $V^2$  as the state variable.  $V^2$  is a monotonic function of the voltage magnitudes. The voltage constraints can still be linear and formulated as (39). The

actual voltage magnitudes can be easily obtained through a square root operation for a given  $V^2$ .

The cosine function becomes the only nonlinear term in the approximated equations. When utilizing the classic assumption,  $\cos \theta'_{ij}$  can be approximated as 1. However, the accuracy becomes worse, especially for reactive power. The significance of retaining the cosine function is illustrated through the following quantitative analysis. The general linear power flow model is:

$$V_i'V_j \sin \theta' \approx \eta_P, \quad (12)$$

$$V_i'^2 - V_i'V_j \cos \theta' \approx \eta_Q, \quad (13)$$

where  $\eta_P$  and  $\eta_Q$  are approximations of the two nonlinear terms in (3) and (4), which are strongly related to active and reactive power respectively because generally  $b_{ij} \gg g_{ij}$  in transmission systems. Two indicators are defined:

$$\varepsilon_P = \int_{\Gamma} (V_i'V_j \sin \theta'_{ij} - \eta_P)^2 dV_i' dV_j d\theta'_{ij} \quad (14)$$

$$\varepsilon_Q = \int_{\Gamma} (V_i'^2 - V_i'V_j \cos \theta'_{ij} - \eta_Q)^2 dV_i' dV_j d\theta'_{ij}, \quad (15)$$

where  $\varepsilon_P$  and  $\varepsilon_Q$  reflect the approximation errors of  $\eta_P$  and  $\eta_Q$  respectively.  $\varepsilon_P$  and  $\varepsilon_Q$  are presented in Table I. The operational region  $\Gamma$  is defined as:

$$\Gamma = \{(V_i', V_j, \theta'_{ij}) | 0.9 \leq V_i' \leq 1.1, 0.9 \leq V_j \leq 1.1, |V_i' - V_j| \leq 0.05, |\theta'_{ij}| \leq \pi/6\}. \quad (16)$$

TABLE I  
ERRORS ( $10^{-5}$ ) OF DIFFERENT APPROXIMATIONS

$\eta_P$	$\varepsilon_P$	$\eta_Q$	$\varepsilon_Q$
		$\frac{V_i'^2 - V_j^2}{2}$	6.8320
$\theta'_{ij}$	1.7786	$\frac{V_i'^2 - V_j^2}{2} - \cos \theta'_{ij} + 1$	0.0715
$\sin \theta'_{ij}$	1.6532	$V_i' - V_j - \cos \theta'_{ij} + 1$	0.0733

The following conclusions can be drawn from Table I: 1) Reactive power exhibits a stronger nonlinearity than active power because 6.8320 is greater than 1.7786 when both approximations ignore nonlinear trig functions. 2) With  $\sin \theta'_{ij}$  retained,  $\varepsilon_P$  reduces slightly. To further improve, the voltage effects should be considered, which is out of scope in this paper and can be explored in the future. 3) With  $\cos \theta'_{ij}$  retained,  $\varepsilon_Q$  reduces significantly. 4) The errors can be further reduced from 0.0733 to 0.0715 if  $V^2$  is used as the independent variable.

Moreover, with  $\cos \theta'_{ij}$  retained, the expression of the branch loss is derived as (17). Although  $P_{ij}^{\text{loss}}$  becomes independent of voltage, a nonnegative loss is guaranteed when  $\cos \theta'_{ij}$  is retained. Otherwise,  $P_{ij}^{\text{loss}}$  will be treated as 0.

$$P_{ij}^{\text{loss}} = P_{ij} + P_{ji} = g_{ij}(V_i'^2 + V_j^2 - 2V_i'V_j \cos \theta'_{ij}) \approx g_{ij}(2 - 2 \cos \theta'_{ij}). \quad (17)$$

Therefore, aiming to enhance the approximation accuracy, it is crucial to reserve the nonlinearity of the cosine functions as much as possible while still rendering tractable optimizations. Hence, a one-dimensional piecewise linearization technique

is employed for  $\cos \theta'_{ij}$ . As shown in Fig. 2, the domain set  $[\underline{\theta}_{ij}, \bar{\theta}_{ij}]$  is partitioned evenly into  $\theta_{ij,k} \in \mathbb{R}$ ,  $k = 0, 1, 2, \dots, N_K$ :

$$\theta_{ij,k} = \underline{\theta}_{ij} + k(\bar{\theta}_{ij} - \underline{\theta}_{ij})/N_K, \quad (18)$$

where  $N_K$  denotes the number of segments. The parameters for the piecewise linearization,  $\underline{\theta}_{ij}$ ,  $\bar{\theta}_{ij}$ ,  $N_K$ , should be selected based on the following rules. First, in order to ensure the optimization problem feasible, the domain set  $[\underline{\theta}_{ij}, \bar{\theta}_{ij}]$  should be large enough. In other words, the set should contain the maximum angle difference of the system. In the pursuit of robustness, the set can be  $[-\pi/4, \pi/4]$  considering that very long lines may exist [4]. Second,  $N_K$  should be selected appropriately considering both approximation accuracy and computation burden. This paper recommends  $N_K \in [20, 50]$  based on the tests in Section IV-A. It should be noted that other partitioning methods, such as the method in [20], can be extended to the proposed piecewise linear approximation. Therefore, a unique interpolation of  $\cos \theta'_{ij}$  can be obtained according to a convex combination of  $\theta_{ij,k}$ :

$$\theta'_{ij} = \sum_{k=0}^{N_K} w_{ij,k} \theta_{ij,k}, \quad (19)$$

$$\cos \theta'_{ij} \approx \sum_{k=0}^{N_K} w_{ij,k} \cos \theta_{ij,k}, \quad (20)$$

$$\sum_{k=0}^{N_K} w_{ij,k} = 1, \quad (21)$$

$$w_{ij,k} \in [0, 1], \quad \forall k = 0, 1, 2, \dots, N_K. \quad (22)$$

The combination of two adjacent breakpoints is illustrated by the black point in Fig. 2. The coefficients  $w_{ij,k}$  are continuous variables, and the sum of  $w_{ij,k}$  should be equal to 1 (21).

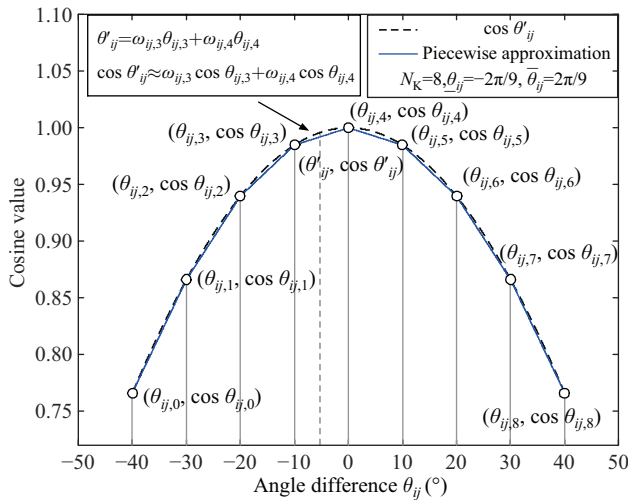


Fig. 2. Schematic diagram of the piecewise linear approximation.

To determine the located segment of  $(\theta'_{ij}, \cos \theta'_{ij})$ , a set of binary variables  $w_{ij,k}$  are introduced. If  $\theta'_{ij} \in [\theta_{ij,k-1}, \theta_{ij,k}]$ , only the corresponding binary variable  $w_{ij,k}$  of the segment is set as 1. Thus, we have the following constraints:

$$\sum_{k=1}^{N_K} w_{ij,k} = 1, \quad (23)$$

$$w_{ij,k} \in \{0, 1\}, \quad \forall k = 1, 2, \dots, N_K. \quad (24)$$

Only the two coefficients  $w_{ij,k-1}, w_{ij,k}$  are nonzero, while the others are all zero. Therefore, the following constraints are included to ensure the adjacent coefficients  $w_{ij,k}$  are nonzero only when the corresponding located segment is activated:

$$w_{ij,0} \leq w_{ij,1}, \quad w_{ij,N_K} \leq w_{ij,N_K}, \quad (25)$$

$$w_{ij,k} \leq w_{ij,k} + w_{ij,k+1}, \quad \forall k = 1, 2, \dots, N_K - 1. \quad (26)$$

By substituting (10), (11) and (20) into (1) and (2), we obtain the piecewise power flow equations:

$$P_i = \sum_{j \in \mathcal{I}_i} \left[ g_{ij} \left( \frac{V_i'^2 - V_j^2}{2} - \sum_{k=0}^{N_K} w_{ij,k} \cos \theta_{ij,k} + 1 \right) - b_{ij} \theta'_{ij} \right] \quad \forall i \in \mathcal{I}, \quad (27)$$

$$Q_i = \sum_{j \in \mathcal{I}_i} \left[ -b_{ij} \left( \frac{V_i'^2 - V_j^2}{2} - \sum_{k=0}^{N_K} w_{ij,k} \cos \theta_{ij,k} + 1 \right) - g_{ij} \theta'_{ij} - b_{ij}^l V_i'^2 / 2 \right] - b_i^{\text{SH}} V_i^2, \quad \forall i \in \mathcal{I}. \quad (28)$$

The independent state variables are the generalized voltage magnitude  $V^2$ , and the phase angle  $\theta$ .  $\cos \theta'_{ij}$  is retained in (27), (28) and approximated by auxiliary continuous variables  $w_{ij,k}$ . Binary variables  $w_{ij,k}$  along with constraints will be introduced into the optimizations. The number of binary variables is  $N_b N_K$ .  $N_b$  denotes the number of branches. The searching space containing the binary variables hinders the optimization solution, especially for large systems.

It is challenging to facilitate optimizations based on piecewise linear power flow models and meanwhile ensure an enhanced approximation accuracy. Essentially, the piecewise models improve the accuracy because of the approximated cosine function  $\sum_{k=0}^{N_K} w_{ij,k} \cos \theta_{ij,k}$ . To address this problem, this paper attempts to ease the evaluation of this approximated cosine function. The details of this concept are presented as follows.

The value of  $\cos \theta'_{ij}$  is obtained based on the angle difference  $\theta'_{ij}$ . The phase angles  $\theta_i, i \in \mathcal{I}$  are the stated variables in the piecewise power flow equations (27) and (28).  $\theta_i$  is coupled with both the active and reactive nodal power injections.

However, the connection between the phase angles  $\theta_i$  and the reactive nodal power injections  $Q_i$  can be decoupled because of the well-known P-Q decoupling characteristics for transmission networks, since  $b_{ij} \gg g_{ij}$ . We can obtain the angle differences with little computation, such as the DC model. Thus, we introduce equations to estimate the angle difference:

$$P_i = \sum_{j \in \mathcal{I}_i} \frac{\theta_{ij}^{\text{PW}}}{x_{ij}} = \sum_{j \in \mathcal{I}_i} \frac{\theta_i^{\text{PW}} - \theta_j^{\text{PW}} - \phi_{ij}}{x_{ij}}, \quad (29)$$

$$\forall i = 1, \dots, N - 1,$$

$$\theta_N^{\text{PW}} = 0, \quad (30)$$

where  $\theta_i^{\text{PW}}$  denotes the voltage phase angle of bus  $i$ , which

is used for piecewise linearization.  $N$  denotes the number of buses. Equation (29) models a lossless network while a nonzero loss is guaranteed in (27). In order to avoid the contradictions between (27) and (29) and to ensure their feasibility, the bus  $N$  is considered as a slack bus whose phase angle is set as 0 (31). The estimated angle differences  $\theta_{ij}^{\text{PW}}$  are only used to determine the convex combination and the coefficient  $w_{ij,k}$ :

$$\theta_{ij}^{\text{PW}} = \sum_{k=0}^{N_K} w_{ij,k} \theta_{ij,k}. \quad (31)$$

Finally, the DPWLPF model is obtained, and the overall constraints include (21)–(31). The nonlinear and non-convex power flow equations are turned into a series of linear constraints with binary variables. The process of piecewise linearization shown in Fig. 2 can be achieved equivalently by linear constraints.  $w_{ij,k}$  and  $u_{ij,k}$  are introduced to optimization problems as auxiliary variables.

Controllable phase-shifting transformers can be modeled in DPWLPF without breaking the linearity. The discrete control characteristics of tap ratios can be precisely and linearly modeled [1]. The phase shift angles are linearly embedded in DPWLPF and can be direct control variables. In this paper, tap ratios and phase shift angles are considered as parameters.

Note that the P-Q decoupling is only utilized in the process of piecewise linearization. In the power flow equations, the coupling between  $V, \theta, P$  and  $Q$  is still considered, which is distinct from the DC model. In other words,  $\theta_i$  are still retained in (27) and (28) and affected by reactive power. Many factors affect the solution time of MILP. In addition to the size, the problem structure is an important factor. The DPWLPF model relieves the computational burden by adjusting the problem structure. It can be observed that  $\theta_{ij}^{\text{PW}}$  only depends on the active nodal power injections. Once  $\theta_{ij}^{\text{PW}}$  is determined, the weight coefficients  $w_{ij,k}$  and binary variables  $u_{ij,k}$  are also determined through the constraints (21)–(26) and (31).  $Q$  and  $V^2$  will not directly affect the approximated cosine function. Thus,  $Q$  and  $\theta_{ij}^{\text{PW}}$  are decoupled. The DPWLPF model reduces the coupling between the variables and still achieves a piecewise linearization.

Because of ignoring the effects of reactive power, the error between  $\theta_{ij}^{\text{PW}}$  and the actual angle differences may increase. Hence, the approximation of piecewise linearization may deteriorate. However, using  $\theta_{ij}^{\text{PW}}$  can still improve accuracy. Power flow calculation is utilized to illustrate the robustness of DPWLPF. The results under different load scales of the IEEE 118 system are compared with the AC solution. Table II shows

the root-mean-square (RMS) errors of voltage magnitudes, the values of  $\cos \theta'_{ij}$  (the approximated cosine function) and DC angle differences of  $\theta_{ij}^{\text{PW}}$ . With the load increasing, the RMS error between  $\theta_{ij}^{\text{PW}}$  and actual angle differences increases. However,  $\cos \theta'_{ij}$  approximated through  $\theta_{ij}^{\text{PW}}$  is still closer to the actual cosine values than 1. Therefore, the voltages obtained by DPWLPF are more accurate than those of the linear model.

To further investigate computational efficiency and accuracy of DPWLPF, numerical tests of OPF under benchmark systems are conducted in Section IV-A.

### III. UNDER VOLTAGE LOAD SHEDDING BASED ON DPWLPF

#### A. Procedure of UVLS

UVLS is an important means to prevent voltage instability. This paper employs LM as the voltage stability criterion. LM denotes the maximum amount of additional load at a given operation point. The flowchart of the proposed UVLS approach is shown in Fig. 3. When a contingency is detected by the online monitor system, after a certain delay, the relay control will shed the load following the predetermined UVLS strategy. Under normal circumstances, the system refreshes the UVLS strategy periodically depending on the online system states. The contingency set is defined by the operators, which can include the  $N - 1$  contingencies and  $N - 2$  contingencies with relatively high probabilities.

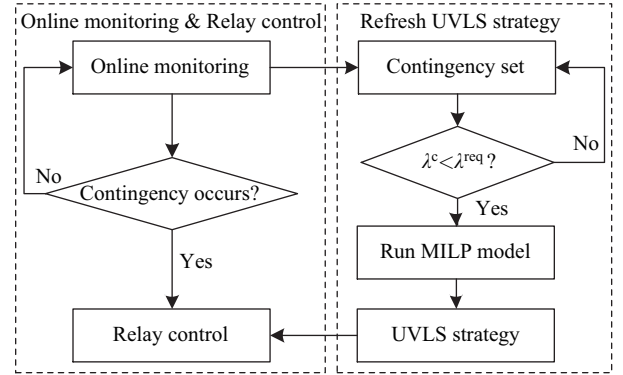


Fig. 3. Flowchart of the proposed UVLS approach.

For each contingency, the post-contingency LM  $\lambda^c$  can be obtained by the optimization-based method [21] based on the power flow snapshot obtained by the online monitor system. If  $\lambda^c$  is smaller than the LM requirement  $\lambda^{\text{req}}$ , the UVLS optimization is solved to generate and refresh the UVLS strategy of contingency  $c$ . The refresh rate is limited by the solution speed of optimizations. Parallel computing techniques can accelerate this process. The UVLS optimization is a MILP-based problem and is introduced in Section III-B. The UVLS strategy, i.e., the optimal solution, determines which feeders should shed load. When a certain contingency occurs, the latest corresponding strategy is adopted by the relay control to ensure LM is satisfying the requirement.

The online monitoring and relay control can be achieved by the supervisory control and data acquisition (SCADA) systems

TABLE II  
THE PERFORMANCE OF DPWLPF UNDER DIFFERENT LOAD SCALES

Model	RMS errors	Load scale			
		1	1.1	1.2	1.3
DPWLPF	Voltage	$3 \times 10^{-4}$	$4 \times 10^{-4}$	$6 \times 10^{-4}$	0.001
	Values of $\cos \theta'_{ij}$	$8 \times 10^{-4}$	0.001	0.003	0.005
	Angle differences	0.007	0.009	0.011	0.016
Linear model*	Voltage	0.002	0.003	0.004	0.005
	Values of $\cos \theta'_{ij}$	0.004	0.007	0.012	0.019

\*: The cosine function in power flow equations is considered as 1

and remote terminal units (RTU). SCADA/RTU have been widely utilized in power systems. Considering the communication speed of SCADA/RTU and the solution time of the optimizations, the refresh period can be about 5 minutes. To ensure the robustness, the load in optimization can be set as the maximum load during the refresh period because the load may fluctuate.

### B. Optimization Problem

The UVLS optimization for contingency  $c$  is formulated as follows:

$$\min \sum_{z \in \mathcal{Z}} C_z x_z^c \quad (32)$$

subject to

$$x_z^c \in \{0, 1\}, \quad \forall z \in \mathcal{Z}, \quad (33)$$

$$(21) - (31), \quad \forall i \in \mathcal{I}. \quad (34)$$

$$P_i = \sum_{g \in i} P_g^c - (1 + \lambda^{\text{req}})(P_i^{\text{D}} - P_i^{\text{shed}}), \quad \forall i \in \mathcal{I}, \quad (35)$$

$$Q_i = \sum_{g \in i} Q_g^c - (1 + \lambda^{\text{req}})(Q_i^{\text{D}} - Q_i^{\text{shed}}), \quad \forall i \in \mathcal{I}, \quad (36)$$

$$\underline{P}_g \leq P_g^c \leq \bar{P}_g, \quad \forall g \in \mathcal{G}, \quad (37)$$

$$\underline{Q}_g \leq Q_g^c \leq \bar{Q}_g, \quad \forall g \in \mathcal{G}, \quad (38)$$

$$\underline{V}_i^2 \leq (V_i^c)^2 \leq \bar{V}_i^2, \quad \forall i \in \mathcal{I}, \quad (39)$$

$$\sqrt{2}S_{ij} \geq P_{ij}^c + Q_{ij}^c \geq -\sqrt{2}S_{ij}, \quad \forall ij \in \mathcal{B}, \quad (40)$$

$$\sqrt{2}S_{ij} \geq P_{ij}^c - Q_{ij}^c \geq -\sqrt{2}S_{ij}, \quad \forall ij \in \mathcal{B}, \quad (41)$$

$$S_{ij} \geq P_{ij}^c \geq -S_{ij}, \quad \forall ij \in \mathcal{B}, \quad (42)$$

$$S_{ij} \geq Q_{ij}^c \geq -S_{ij}, \quad \forall ij \in \mathcal{B}. \quad (43)$$

The objective function is to minimize the total cost of load curtailment (32). Binary variables  $x_z^c$  denote the load shedding strategy (33).  $x_z^c$  is equal to 1 if all the load at feeder  $z$  is shed and 0 otherwise. Note that continuously controllable loads can be easily extended in this model. The constraints of the DPWLPF modeling presented in Section II are included to provide a picture of post-contingency system states after UVLS (34). The nodal power balance equations are described as (35) and (36). The output active and reactive powers for the units should be limited in the allowable range (37), (38). The voltage magnitudes of buses are restricted in the security range (39). Constraints (40)–(43) represent the piecewise linear quadratic apparent branch flow constraints [22].

### C. ZIP Load Modeling

The ZIP model is used to depict the voltage-dependent nonlinear load characteristics:

$$P_i^{\text{D}} = P_i^0 [a_i^{\text{Z}}(V_i^c)^2 + a_i^{\text{I}}V_i^c + a_i^{\text{P}}], \quad (44)$$

$$Q_i^{\text{D}} = Q_i^0 [a_i^{\text{Z}}(V_i^c)^2 + a_i^{\text{I}}V_i^c + a_i^{\text{P}}], \quad (45)$$

where  $a_i^{\text{Z}}, a_i^{\text{I}}, a_i^{\text{P}}$  are the proportion coefficients for ZIP load modeling. Since  $(V_i^c)^2$  is the independent state variable of DPWLPF,  $V_i^c$  in (44) and (45) becomes a nonlinear term.  $V_i^c$  can be linearized as  $0.5(V_i^c)^2 + 0.5$  around the nominal operation point. Hence, equations (46) and (47) become linear:

$$P_i^{\text{D}} = P_i^0 [(a_i^{\text{Z}} + 0.5a_i^{\text{I}})(V_i^c)^2 + 0.5a_i^{\text{I}} + a_i^{\text{P}}], \quad (46)$$

$$Q_i^{\text{D}} = Q_i^0 [(a_i^{\text{Z}} + 0.5a_i^{\text{I}})(V_i^c)^2 + 0.5a_i^{\text{I}} + a_i^{\text{P}}]. \quad (47)$$

Similarly, the amount of active and reactive load shedding of bus  $i$  can be calculated by (48) and (49). In this paper, the proportion coefficients of different feeds located at a same bus are assumed as consistent.

$$P_i^{\text{shed}} = \sum_{z \in i} P_z^{\text{shed},0} [(a_i^{\text{Z}} + 0.5a_i^{\text{I}})(V_i^c)^2 + 0.5a_i^{\text{I}} + a_i^{\text{P}}] x_z, \quad (48)$$

$$Q_i^{\text{shed}} = \sum_{z \in i} Q_z^{\text{shed},0} [(a_i^{\text{Z}} + 0.5a_i^{\text{I}})(V_i^c)^2 + 0.5a_i^{\text{I}} + a_i^{\text{P}}] x_z. \quad (49)$$

There is a bilinear term  $(V_i^c)^2 x_z$ . Auxiliary constraints are included to turn the bilinear term into linear:

$$-\bar{V}_i^2(1 - x_z) + (V_i^c)^2 \leq \mu_z \leq (V_i^c)^2, \quad (50)$$

$$V_i^2 x_z \leq \mu_z \leq \bar{V}_i^2 x_z. \quad (51)$$

Moreover,  $\mu_z$  should replace  $(V_i^c)^2 x_z$  in (48) and (49).

## IV. CASE STUDIES

Case studies are conducted on a computer with an Intel Core i7-8550U CPU at 1.80 GHz and 15.9 GB of RAM. The MILP solver is GUROBI 8.1 [23]. The optimality gap tolerance is set as 0.01%. The parameters for the piecewise linearization  $\underline{\theta}_{ij}, \bar{\theta}_{ij}, N_K$ , are set as  $-\pi/6, \pi/6$  and 24 respectively.

### A. Numerical Tests of OPF

The effects of the proposed decoupled piecewise power flow modeling are discussed in Section II-B. The actual performance should be investigated through numerical tests. Here, we use the fundamental optimization in power systems, OPF, as the testing platform. To verify the effectiveness of DPWLPF, three other power flow modeling schemes along with DPWLPF are tested under several benchmark systems:

*Scheme 1:* The cosine functions are approximated as 1 in the proposed linearization (10), (11).

*Scheme 2:* The cosine functions are approximated by the conventional piecewise modeling method. The functions are determined by  $\theta'_{ij}$  in the power flow equations (27), (28), which are coupled with both active and reactive power.

*Scheme 3:* The cosine functions are retained by the proposed decoupled piecewise modeling method. However,  $V$  instead of  $V^2$  is considered as the independent variable.

*Scheme 4:* The proposed DPWLPF.

Because the cosine functions are globally considered as 1, OPF based on scheme 1 are linear programming problems. OPF based on other schemes are MILP problems. The results are compared with ACOF. The solution time and absolute gap of objectives are shown in Table III. Detailed data of these systems can be obtained from the package of MATPOWER [24]. The cost of reactive power generation is considered as 10% of that of active generation. S1–S4 are short for the four modeling schemes. It can be observed that the solution of all modeling schemes is rapid for small systems. S1 owns the fastest solution efficiency. The solution time is 1.22 s even for the largest system. However, the solution time of S2

TABLE III  
SOLUTION TIME AND ABSOLUTE GAP OF OBJECTIVES

System	Solution time (s)				Absolute gap (%)			
	S1	S2	S3	S4	S1	S2	S3	S4
IEEE 9	0.01	0.02	0.01	0.02	4.65	0.53	1.02	0.97
IEEE 30	0.03	0.06	0.05	0.06	11.6	4.11	1.94	1.96
IEEE 118	0.07	0.59	0.61	0.67	2.84	0.10	0.25	0.25
IEEE 300	0.18	1.95	1.58	1.61	2.88	0.13	0.92	0.89
PEGASE 1354	0.78	206	70.5	60.1	2.56	1.65	1.56	1.55
POLISH 2383wp	1.22	1723	1349	1147	5.54	3.66	3.76	3.69

increases markedly especially for relatively large systems, i.e., PEGASE 1354 and POLISH 2382wp. Because of piecewise linearization, the size of optimizations is enlarged. The binary variables are too many to provide an efficient solution for S2. S3 and S4 employ the proposed decoupled piecewise modeling method and adjust the problem structure. Although the number of binary variables is the same compared with S2, the solution time of large systems still decreases significantly.

To further compare the approximation accuracy of system states, we calculate the RMS errors of voltage magnitudes and branch apparent power flows between ACOPF and OPF based on the approximated models. For easy visualization, the RMS errors are normalized as shown in Fig. 4. The RMS errors of S1 are considered as the baselines. It can be observed that the errors of S1 are larger than the errors of the other three modeling schemes. As analyzed before, the cosine functions are important to approximate the reactive power equations. The piecewise linearization of the cosine functions has a positive effect on approximation. Moreover, the network loss can be considered leading to reduced errors of branch flows for S2, S3 and S4.

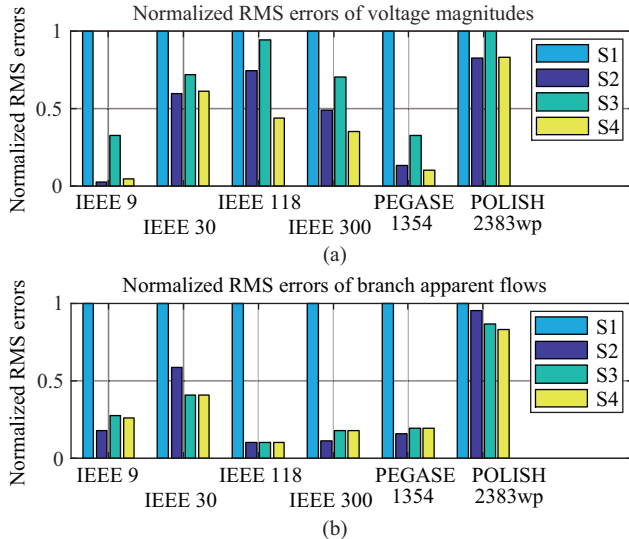


Fig. 4. Normalized RMS errors of (a) voltage magnitudes; (b) branch apparent flows.

However, none of the three piecewise models dominates the others in approximation accuracy. The more precise modeling schemes considering different indicators are shown in Fig. 5. Statistically, S2 is the more precise modeling scheme because 61% of the quantities obtained by S2 are more accurate than

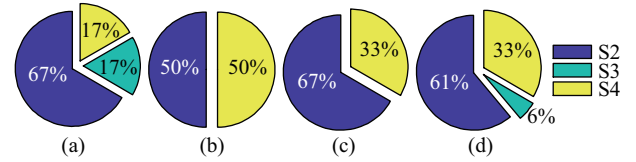


Fig. 5. The scenario ratio of the most precise modeling scheme considering (a) Absolute gap between objectives; (b) Voltage magnitudes; (c) Branch flows; (d) All of the above quantities.

the others. However, the computational burden of S2 is heavy for large systems as shown in Table II. For S3, the ratio in Fig. 5 is less than the other two piecewise modeling schemes. In addition, the RMS errors are obviously greater in some cases, such as the voltage magnitudes of IEEE 9, which indicates using  $V^2$  as the independent variable can enhance the approximation.

The effect on accuracy of the decoupled piecewise modeling method is observed here. The RMS errors of S4 are close to those of S2. Using the proposed decoupled modeling method may reduce the accuracy slightly. But in some cases, the accuracy is improved, i.e., 33% of quantities obtained by S4 are more precise. Given the increase in computational efficiency, S4 achieves a better trade-off between approximation accuracy and computational efficiency.

The RMS errors of voltage magnitudes and solution time for the PEGASE 1354 system under different values of  $N_K$  are shown in Fig. 6. Because of the symmetry of the cosine function in the given  $[\underline{\theta}_{ij}, \bar{\theta}_{ij}]$ , we set  $N_K$  as different even numbers. It can be observed that if  $N_K$  is too small, the error is large. With  $N_K$  increasing, the error decreases. However, when  $N_K$  is large enough, the error hardly decreases, while the solution time tends to increase significantly. Hence, we recommend  $N_K \in [20, 50]$  to achieve a tradeoff between errors and solution time.

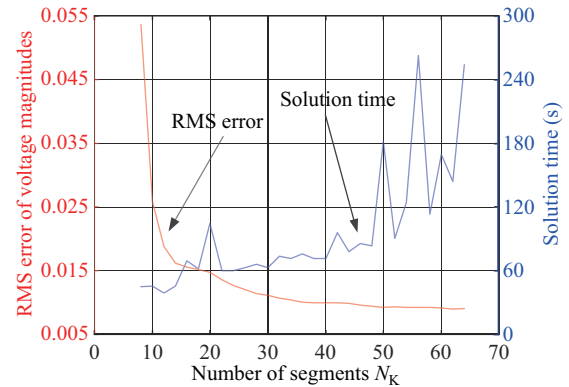


Fig. 6. Performance under different numbers of segments.

### B. Performance of UVLS

The proposed UVLS method is implemented in the IEEE 118 system. The LM requirement  $\lambda^{\text{req}}$  after a contingency is set as 0.05. The proportion coefficients of ZIP load  $a_i^Z, a_i^I, a_i^P$  are assumed as 0.25, 0.25, 0.5 respectively. We increase the load by 30% and reduce the generation capacity by 40% to simulate a heavy loading scenario. For each bus with nonzero load, there are three feeders for potential load curtailment.

Suppose the system is disturbed by a severe  $N - 2$  contingency, which is defined as the simultaneous outage of the generator located at bus 12 and the lines 27–28. The corresponding post-contingency LM  $\lambda^c = 0.0024$  of this  $N - 2$  contingency is less than  $\lambda^{\text{req}}$ . The UVLS strategy of the power flow snapshot is already generated by the optimization presented in Section III-B beforehand. Hence, the relay control sheds the load according to the predetermined strategy.

According to the theorem in [21], the type of bifurcation observed in this case is the so-called limit induced bifurcation, which is illustrated by the PV curves shown in Fig. 7. In a normal situation, the voltage of bus 1 is maintained as 0.94 p.u. When the equilibrium point moves from O to A with the load increasing, the reactive power outputs of the generators also increase. When the point reaches A, the generator located at bus 1 generates maximum reactive power. The blue curve indicates the PV curve when the generator located at bus 1 always generates maximum reactive power output. The point A is below the saddle node and means the voltage collapses. The pre-contingency LM  $\lambda^n = 0.0547$  is the length of the OA. If the  $N - 2$  contingency occurs, the maximum load point will move from point A to B, as shown in Fig. 7. In addition, LM will reduce to 0.0024, which is far less than the LM requirement. The system faces the risk of voltage instability. However, if the relay control system sheds the load located at the assigned feeders following the UVLS strategy, the base equilibrium point of the system will move from O to M. And LM becomes  $\lambda^{\text{UVLS},c} = 0.0491$ , which is quite close to the requirement  $\lambda^{\text{req}} = 0.05$ .

There are inevitable errors in linear approximated power flow models. Therefore, either over-optimistic or conservative solutions may be obtained by the MILP-based UVLS optimization. This paper recommends operators determine the higher LM requirement to avoid security risks considering load fluctuation between the refresh interval, load modeling errors and approximation accuracy.

To further verify the effectiveness of the proposed UVLS based on DPWLPF, the results are compared under different power flow models and different contingencies. The contingency set is defined as the loss of a single generator and single line outage. Based on the procedure shown in Fig. 3, we can sort out severe contingencies. Because the load is heavy, a total of 76 contingencies are diagnosed as severe contingencies and their LMs cannot satisfy the requirement.

Then the UVLS strategies are obtained by optimizations based on different power flow models. The four modeling schemes from Section IV-A are employed here. In addition, the AC power flow modeling is utilized here as scheme 5. However, the optimization problem is a MINLP, which is intractable for many solvers. Therefore, binary variables  $x_z^c$  are considered as continuous variables by adding auxiliary constraints  $x_z^c(1 - x_z^c) = 0$ . And the original MINLP problem becomes nonlinear programming (NLP), which can be solved by IPOPT [25].

The performance of UVLS strategies obtained by different power flow models can be evaluated by the mean absolute error of LM, which is defined as:

$$\text{MAE} = \sum_{c \in \mathcal{C}^*} \frac{|\lambda^{\text{UVLS},c} - \lambda^{\text{req}}|}{\text{card}(\mathcal{C}^*)}, \quad (52)$$

where  $\mathcal{C}^*$  denotes the set of severe contingencies and  $\text{card}(\mathcal{C}^*)$  denotes the number of severe contingencies. The smaller MAE is, the better the quality of the solution is. The MAE of different models are shown in Table IV. Note S5 is not available here. The NLP problem is diagnosed as infeasible or the number of iterations exceeds the maximum limit. Furthermore, the LMs after the UVLS of different contingencies are shown in Fig. 8. The contingencies are sorted by severity degree. Through UVLS, the LM can be improved. However, the MAE of S1 is significantly larger than the MAE of other schemes because ignoring the nonlinearity of the cosine function leads to lower accuracy. Moreover, S1 estimates LM over-optimistically and sheds less load for lower cost. The LMs after the UVLS of S1 are shown as the red curve in Fig. 8. Some of them are obviously less than the requirement. By the piecewise linearization, the LMs of S2, S3 and S4 are close to the requirement. What's more, the actual voltages at the maximum load point are compared with those obtained by optimization. The RMS errors of the voltage

TABLE IV  
PERFORMANCE OF UVLS STRATEGIES OBTAINED BY DIFFERENT MODELS

Scheme	MAE ( $10^{-3}$ )	RMS error of voltages
S1	9.18	0.0225
S2	3.19	0.0107
S3	3.97	0.0132
S4	2.92	0.0104
S5	N/A	N/A

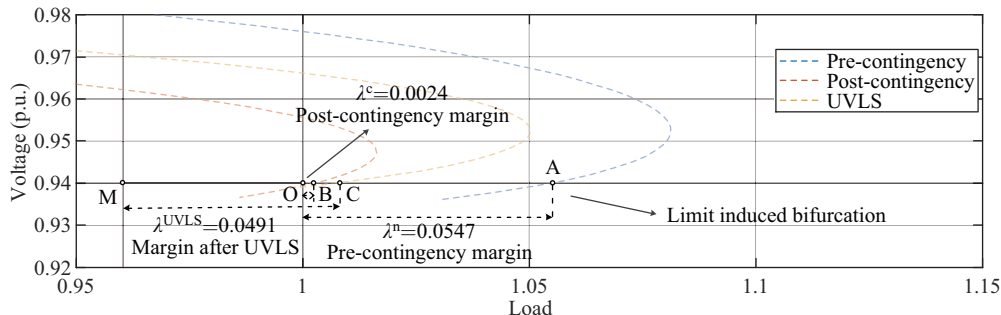


Fig. 7. PV curves under pre-contingency configuration, under post-contingency configuration and after UVLS.

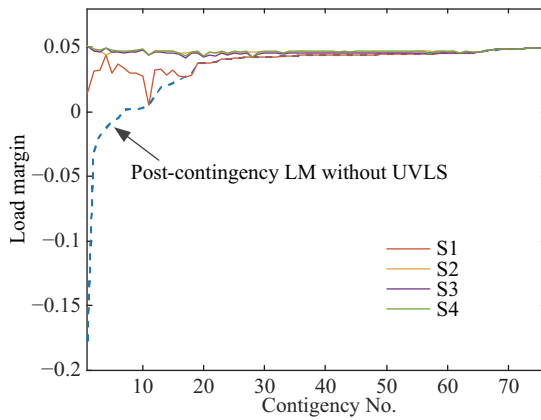


Fig. 8. LMs of contingencies after UVLS obtained by different modeling schemes.

magnitudes under the four schemes are presented in Table IV respectively. S4 provides the most accurate picture of voltage profiles indicating the proposed DPWLPF is the most accurate modeling scheme in this case. Hence, the MAE of S4 is the smallest, i.e., the UVLS strategy obtained by S4 outperforms the others.

A Monte Carlo simulation is conducted for the IEEE 118 system to investigate the performance of UVLS under load fluctuation during the refresh period. The load is assumed to be distributed uniformly with a certain deviation ratio from the base value, e.g.  $P_i^0 \sim U(0.95P_i^0, 1.05P_i^0)$ . For each deviation ratio that belongs to  $\{0.01, 0.02, 0.03, 0.04, 0.05\}$ , 5,000 random scenarios are simulated. The load fluctuates while the predefined UVLS strategy is the same and executed after the outage of lines 76–77. To improve robustness, the load in optimization increases by 3%. The LMs after UVLS are shown in Fig. 9. At 5% fluctuation, sufficient margin of voltage stability can still be guaranteed, i.e.,  $\lambda^{\text{UVLS,c}} > 0.05$ .

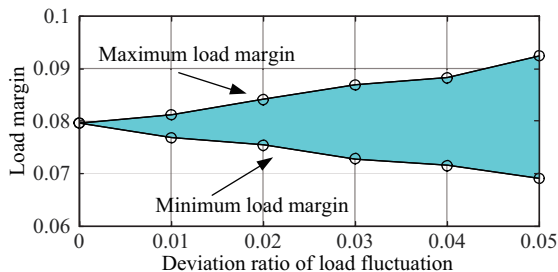


Fig. 9. LMs after UVLS under load fluctuation.

The average solution time of all three piecewise models is around 1 s. To further compare the computational speed, a case study is conducted for a larger system, PEGASE 1354. The average solution time of the models is 271 s, 141 s and 136 s respectively, which verifies that the proposed decoupled piecewise modeling approach relieves the computational burden.

## V. CONCLUSION

This paper proposes a piecewise linear power flow model called DPWLPF. Aiming at improving the computational efficiency, a decoupled modeling method is proposed to decouple

the reactive power and approximated cosine functions in piecewise power flow equations.

Through case studies under benchmark systems, DPWLPF effectively relieves the computational burden, especially for large systems, while not significantly impairing the approximation of the piecewise linearization. Approximation accuracy may reduce slightly. But in some cases, accuracy improves.

Based on DPWLPF, an UVLS approach is presented. DPWLPF can turn the intractable MINLP problem into MILP. LM is improved by the generated UVLS strategy to avoid static voltage instability. Moreover, DPWLPF has the potential to be augmented for other intractable MINLP problems in power systems, which can be explored in a future study.

## REFERENCES

- [1] Z. F. Yang, H. W. Zhong, A. Bose, Q. Xia, and C. Q. Kang, "Optimal power flow in AC–DC grids with discrete control devices," *IEEE Transactions on Power Systems*, vol. 33, no. 2, pp. 1461–1472, Mar. 2018.
- [2] T. Akbari and M. TavakoliBina, "Approximated MILP model for AC transmission expansion planning: global solutions versus local solutions," *IET Generation, Transmission & Distribution*, vol. 10, no. 7, pp. 1563–1569, May 2016.
- [3] T. Akbari and M. Tavakoli Bina, "Linear approximated formulation of AC optimal power flow using binary discretization," *IET Generation, Transmission & Distribution*, vol. 10, no. 5, pp. 1117–1123, Apr. 2016.
- [4] B. Stott, J. Jardim, and O. Alsac, "DC power flow revisited," *IEEE Transactions on Power Systems*, vol. 24, no. 3, pp. 1290–1300, Aug. 2009.
- [5] P. A. Trodden, W. A. Bukhsh, A. Grothey, and K. I. M. McKinnon, "Optimization-based islanding of power networks using piecewise linear AC power flow," *IEEE Transactions on Power Systems*, vol. 29, no. 3, pp. 1212–1220, May 2014.
- [6] F. R. Badal, P. Das, S. K. Sarker, and S. K. Das, "A survey on control issues in renewable energy integration and microgrid," *Protection and Control of Modern Power Systems*, vol. 4, pp. 8, Apr. 2019.
- [7] F. D. Xu, Q. L. Guo, H. B. Sun, B. M. Zhang, and L. Jia, "A two-level hierarchical discrete-device control method for power networks with integrated wind farms," *Journal of Modern Power Systems and Clean Energy*, vol. 7, no. 1, pp. 88–98, Jan. 2019.
- [8] D. L. Zhang, J. L. Li, and D. Hui, "Coordinated control for voltage regulation of distribution network voltage regulation by distributed energy storage systems," *Protection and Control of Modern Power Systems*, vol. 3, pp. 3, Jan. 2018.
- [9] G. Mu, J. Wang, and G. G. Yan, "The mechanism of DFIGs grouping tripped off from power grid," *CSEE Journal of Power and Energy Systems*, vol. 4, no. 1, pp. 103–111, Mar. 2018.
- [10] S. M. Fatemi, S. Abedi, G. B. Gharehpetian, S. H. Hosseini, and M. Abedi, "Introducing a novel DC power flow method with reactive power considerations," *IEEE Transactions on Power Systems*, vol. 30, no. 6, pp. 3012–3023, Nov. 2015.
- [11] J. W. Yang, N. Zhang, C. Q. Kang, and Q. Xia, "A state-independent linear power flow model with accurate estimation of voltage magnitude," *IEEE Transactions on Power Systems*, vol. 32, no. 5, pp. 3607–3617, Sep. 2017.
- [12] Y. Wang, N. Zhang, H. Li, J. W. Yang, and C. Q. Kang, "Linear three-phase power flow for unbalanced active distribution networks with PV nodes," *CSEE Journal of Power and Energy Systems*, vol. 3, no. 3, pp. 321–324, Sep. 2017.
- [13] Y. X. Liu, N. Zhang, Y. Wang, J. W. Yang, and C. Q. Kang, "Data-driven power flow linearization: a regression approach," *IEEE Transactions on Smart Grid*, vol. 10, no. 3, pp. 2569–2580, May 2019.
- [14] M. Hohmann, J. Warrington, and J. Lygeros, "Optimal linearizations of power systems with uncertain supply and demand," *IEEE Transactions on Power Systems*, vol. 34, no. 2, pp. 1504–1512, Mar. 2019.
- [15] S. Bahrami and V. W. S. Wong, "Security-constrained unit commitment for AC–DC grids with generation and load uncertainty," *IEEE Transactions on Power Systems*, vol. 33, no. 3, pp. 2717–2732, May 2018.

- [16] O. W. Akinbode and K. W. Hedman, "Fictitious losses in the DCOFP with a piecewise linear approximation of losses," in *Proceedings of 2013 IEEE Power & Energy Society General Meeting*, Vancouver, 2013, pp. 1–5.
- [17] Q. P. Wang, Z. Q. Bo, Y. K. Zhao, X. W. Ma, M. Zhang, H. Zheng, and L. Wang, "Integrated wide area protection and control for power grid security," *CSEE Journal of Power and Energy Systems*, vol. 5, no. 2, pp. 206–214, Jun. 2019.
- [18] J. H. Wang, H. Y. Zhang, and Y. Zhou, "Intelligent under frequency and under voltage load shedding method based on the active participation of smart appliances," *IEEE Transactions on Smart Grid*, vol. 8, no. 1, pp. 353–361, Jan. 2017.
- [19] I. Kaffashan and T. Amraee, "Probabilistic under voltage load shedding using point estimate method," *IET Generation, Transmission & Distribution*, vol. 9, no. 15, pp. 2234–2244, Nov. 2015.
- [20] L. Wu, "A tighter piecewise linear approximation of quadratic cost curves for unit commitment problems," *IEEE Transactions on Power Systems*, vol. 26, no. 4, pp. 2581–2583, Nov. 2011.
- [21] R. J. Avalos, C. A. Canizares, F. Milano, and A. J. Conejo, "Equivalency of continuation and optimization methods to determine saddle-node and limit-induced bifurcations in power systems," *IEEE Transactions on Circuits and Systems I: Regular Papers*, vol. 56, no. 1, pp. 210–223, Jan. 2009.
- [22] X. Chen, W. C. Wu, and B. M. Zhang, "Robust restoration method for active distribution networks," *IEEE Transactions on Power Systems*, vol. 31, no. 5, pp. 4005–4015, Sep. 2016.
- [23] GUROBI Website, 2019. [Online]. Available: <https://www.gurobi.com>.
- [24] R. D. Zimmerman, C. E. Murillo-Sánchez, and R. J. Thomas, "MATPOWER: steady-state operations, planning, and analysis tools for power systems research and education," *IEEE Transactions on Power Systems*, vol. 26, no. 1, pp. 12–19, Feb. 2011.
- [25] A. Wächter and L. T. Biegler, "On the implementation of an interior-point filter line-search algorithm for large-scale nonlinear programming," *Mathematical Programming*, vol. 106, no. 1, pp. 25–57, Mar. 2006.



**Hongbin Sun** (SM'12–F'18) received the B.S. degree in Electrical Engineering from Tsinghua University, Beijing, China, in 1992, and the Ph.D. degree in Electrical Engineering from Tsinghua University, in 1997.

From 2007 to 2008, he was a Visiting Professor with the School of Electrical Engineering and Computer Science, Washington State University, Pullman, WA, USA. He was with Tsinghua University, where he led a research group to develop a commercial system-wide automatic voltage control system, which has been applied to more than 100 electrical power control centers in China and the control center of PJM interconnection, the largest regional power grid in the USA. He has authored or coauthored more than 300 peer-reviewed papers. He is currently a Changjiang Scholar Chair Professor of Education for the Ministry of China, a Tenured Full Professor of Electrical Engineering, and the Director of Energy Management and Control Research Center with Tsinghua University.

Dr. Sun is a fellow of IEEE and IET. He is serving as the Chair for the IEEE Smart Grid Voltage Control Task Force and IEEE Energy Internet Working Group. He served as the Founding Chair for the IEEE Conference on Energy Internet and Energy System Integration in 2017. His current research interests include energy management system, automatic voltage control, energy Internet and multi-energy systems.



**Huaichang Ge** received the B.S. and Ph.D. degrees in Electrical Engineering from Tsinghua University, Beijing, China, in 2013 and 2018, respectively. Dr. Ge is current a Post Doctor with the Department of Electrical Engineering, Tsinghua University. His research interests include voltage stability and voltage control.



**Mang Jiang** received the B.S. degree in Electrical Engineering from Tsinghua University, Beijing, China, in 2017. He joined the State Key Laboratory of Power Systems in September 2017, where he is currently pursuing the Ph.D. degree. His research interests include reactive power optimization and voltage control.



**Qinglai Guo** (SM'14) received the B.S. degree in Electrical Engineering from Tsinghua University, Beijing, China, in 2000, and the Ph.D. degree from Tsinghua University in 2005.

He is currently an Associate Professor with Tsinghua University. He is now an IEEE senior member and a CIGRE member, and is involved in 5 workgroups of these two organizations. His research interests include energy management system, voltage stability and control, and cyber-physical system.